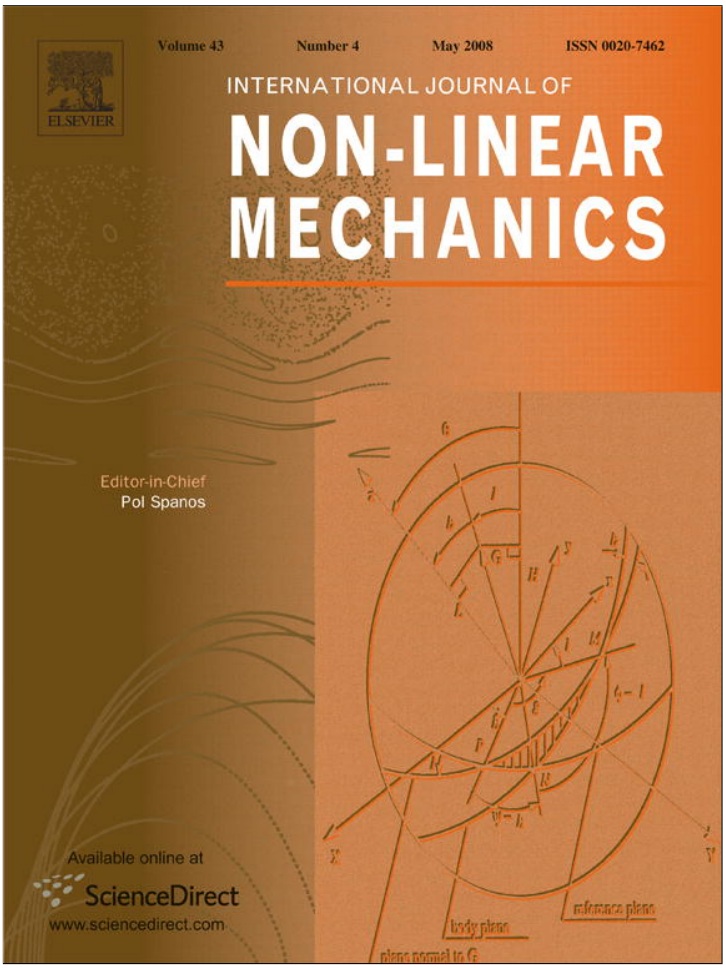

Available online at www.sciencedirect.com
ScienceDirect
International Journal of Non-Linear Mechanics 43 (2008) 277–291
INTERNATIONAL JOURNAL OF NON-LINEAR MECHANICS
www.elsevier.com/locate/nlm

Feedback stabilization of snap-through buckling in a preloaded two-bar linkage with hysteresis☆

Ashwani K. Padthe, Nalin A. Chaturvedi, Dennis S. Bernstein*, Sanjay P. Bhat, Anthony M. Waas

Department of Aerospace Engineering, The University of Michigan, Ann Arbor, MI 48109-2140, USA

Received 2 May 2007; accepted 12 December 2007

Abstract

We study a linearly damped preloaded two-bar linkage that exhibits hysteresis due to the presence of multiple attracting equilibria. The dynamics at the unstable equilibrium, through which a snap-through buckle occurs, are not linearizable due to a solution-dependent singularity. We stabilize the unstable equilibrium using two distinct non-linear controllers. The feedback-linearization controller requires knowledge of the linkage parameters, whereas the robust version of the intrinsic non-linear proportional-derivative controller requires only an upper bound on the stiffness.

Keywords: Buckling; Hysteresis; Robust control

1. Introduction

The phenomenon of hysteresis is widespread and extensively studied [1,2]. Although hysteresis arises in diverse applications, all hysteretic phenomena have a common origin. Specifically, hysteresis is the low-frequency limit of the dynamic input–output response of a system when this limit is a non-degenerate loop [3]. A necessary condition for a system to exhibit hysteresis is the existence of multiple attracting equilibria for a given constant input [4–6]. This statement is the *principle of multistability*.

The principle of multistability implies that any system with multiple equilibria is possibly hysteretic. In structural mechanics, the phenomenon of buckling is closely associated with multiple equilibria, which arise when the axial load applied to a structure counteracts the stiffness of the structure [7]. Consequently, hysteresis can potentially arise when a structure passes through buckling, and this possibility is the motivation for the present paper. Although hysteresis is closely associated with energy dissipation [8], the hysteresis we consider is not a consequence of a hysteretic energy-dissipation mechanism, but rather is due to the multiple equilibria arising from buckling. In fact, the damping model we assume is linear and viscous, which cannot give rise to hysteresis in linear or non-linear structures that possess a unique equilibrium.

In many applications, buckling can lead to structural failure, and thus the usual objective is to avoid conditions under which buckling might occur [9]. There are, however, useful aspects of buckling. For example, buckled elements have been considered for vibration isolation, where the axial and transverse motions have widely different stiffnesses [10,11]. Another application is in mechanical actuators, where the structural dynamics near buckling provide significant mechanical advantage [12,13].

In the present paper we study the preloaded two-bar linkage shown in Fig. 1, which serves as a lumped analogue of a structure that can undergo snap-through buckling, see [32], p. 35. The word preloaded refers to the force provided by the stiffness k when the bars are in the horizontal equilibrium. The preloaded two-bar linkage exhibits the essential features of snap-through buckling, in which a perturbation from the horizontal equilibrium results in a sudden, fast response toward a stable equilibrium.

The two-bar linkage is a kinematically redundant mechanism [14–18]. Kinematic redundancy entails additional degrees

☆ This research was supported in part by the National Science Foundation under Grant ECS-0225799.
* Corresponding author. Tel.: +1 734 764 3719; fax: +1 734 763 0578.
E-mail addresses: akpadthe@umich.edu (A.K. Padthe), nalin@umich.edu (N.A. Chaturvedi), dsbaero@umich.edu (D.S. Bernstein), dcw@umich.edu (S.P. Bhat).

0020-7462/$ - see front matter © 2008 Elsevier Ltd. All rights reserved.
doi:10.1016/j.ijnonlinmec.2007.12.010

of freedom that have no direct impact on meeting task-space objectives but provide advantages in terms of constraint and limit avoidance. In this case, the coefficient of the highest-order derivative has a non-square Jacobian leading to non-unique motions for realizing a given task; in fact, joint motion within the Jacobian's (non-trivial) null space does not affect the trajectory of the end-effector, and thus the inverse kinematics are not unique. The non-unique motions can be chosen to satisfy a subtask or can be specified in terms of the generalized inverse of the Jacobian [19]. The preloaded two-bar linkage possesses a kinematic singularity since, for $\theta = 0$, zero velocity in task space (that is, $\dot{q} = 0$) does not correspond to a unique velocity $\dot{\theta}$ in joint space.

Under the approximating assumption that the bars are inertialess, the two-bar linkage has the property that the inertia is singular at the unstable (horizontal) equilibrium, thereby combining instability with singular dynamics. Inertia singularities arise in linearized vibration theory when certain modes are viewed as inertialess [20,21]. If a structure is nearly inertialess, then classical singular perturbation techniques can be used to approximate the solution in the vicinity of the singularity. More generally, singularities that depend on a fixed, small parameter have been widely studied in the control literature [22]. Furthermore, singular coefficients that multiply the highest-order derivative and that are functions of the *independent* (time or spatial) variable have been extensively studied in the classical dynamical systems literature (see, for example, [23, Chapter V]). The connection between singularities and hysteresis is explored in [24]. In contrast, the singularity in the linkage dynamics (4.1) is solution dependent rather than independent-variable dependent, and thus is not addressed by the classical singular perturbation literature.

The contents of the paper are as follows. In Section 2, we present the two-bar preloaded linkage and determine its equilibria through static analysis. We also derive the static equilibria using energy methods, which help in determining the stability of the equilibria and defining the equilibrium set $\mathscr{E}$ for the preloaded two-bar linkage. Next, in Section 3, we derive the equations of motion with a force input. The resulting equation, whose multiple equilibria are precisely the equilibria obtained from static analysis, possesses a state-dependent inertia singularity at the unstable, horizontal equilibrium. In Section 4 we show that the dynamics are not linearizable at the unstable horizontal equilibrium. Consequently, we derive a small-angle model and obtain a closed-form expression for the free response from an initial non-zero perturbation. In Section 5 we show the existence of non-unique solutions departing from the unstable equilibrium. In Section 6 we demonstrate hysteresis in the preloaded two-bar linkage. We also show that the hysteresis map is a subset of the equilibrium set $\mathscr{E}$.

In Section 7 we present control strategies for stabilizing the unstable equilibrium. We first apply a feedback linearizing controller that renders the equilibrium asymptotically stable. Finally, to reduce dependence on the linkage parameters, in Section 8 we apply the intrinsic non-linear proportional-derivative (INPD) controller of [25], which stabilizes the equilibrium by exploiting the structure of the dynamics. A preliminary version of the results in this paper appeared in [26].

2. Static analysis of a preloaded two-bar linkage

In this section we analyze the statics of the preloaded two-bar linkage with joints P, Q, and R and preloaded by a stiffness k as shown in Fig.‘1. A constant vertical force F is applied at Q, where the two bars are joined by a frictionless pin. Let θ denote the counterclockwise angle that the left bar makes with the horizontal, and let q denote the distance between the joints P and R. When $F=0$, the linkage has three equilibrium configurations.

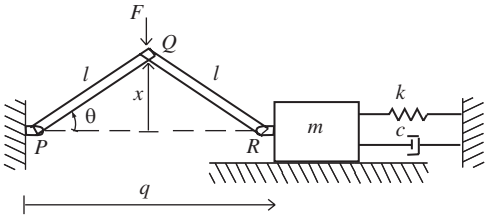

Fig. 1. The preloaded two-bar linkage with a vertical force F acting at the joint Q. The word ‘preloaded’ refers to the presence of the stiffness k, which is compressed when the two-bar linkage is in the horizontal equilibrium.

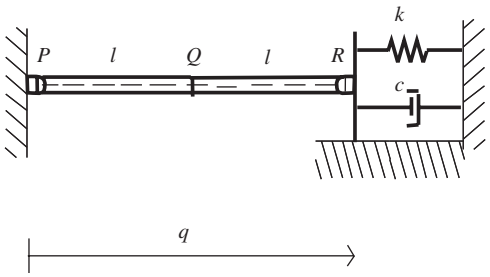

Fig. 3. Static equilibrium with $F=0$ and $\theta=0$. This equilibrium is unstable.

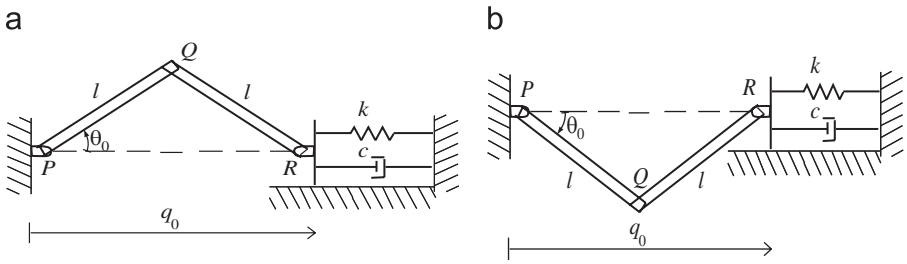

Fig. 2. Static equilibria of the preloaded two-bar linkage when the spring is relaxed and $F=0$. In (a) the equilibrium angle θ_0 is positive, whereas in (b) the angle θ_0 is negative.

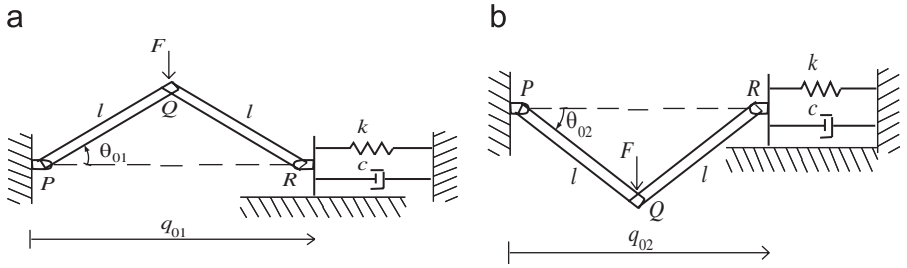

Fig. 4. Static equilibria for the two-bar linkage with a constant force F acting at joint Q. In (a) the equilibrium angle θ_{01} is positive and the spring is compressed, whereas in (b) the equilibrium angle θ_{02} is negative and the spring is extended.

In Fig. 2, the values of q and θ are q_0 and $\pm\theta_0$, respectively, and the spring k is relaxed. Note that $q_0 = 2l\cos\theta_0$. For the third equilibrium shown in Fig. 3, both bars are horizontal with $\theta = 0$.

For a constant non-zero applied force F, the preloaded two-bar linkage has two equilibrium configurations as shown in Fig. 4. In Fig. 4(a) the equilibrium angle θ_{01} is positive and the spring is compressed, whereas in 4(b) the equilibrium angle θ_{02} is negative and the spring is extended. To analyze the equilibrium position shown in Fig. 4, let C_1 and C_2 be the compressive forces in the bars QR and PQ, respectively. Balancing the forces at Q yields

$$C_1\cos\theta = C_2\cos\theta,$$
$$F = C_1\sin\theta + C_2\sin\theta,$$

which implies that

$$F = 2C_1\sin\theta = 2C_2\sin\theta. \tag{2.1}$$

Now, balancing the forces at R yields

$$C_1\cos\theta = k(q - q_0). \tag{2.2}$$

Substituting $q = 2l\cos\theta$ and using (2.1), we obtain

$$(\sin\theta)\left(1 - \frac{\cos\theta_0}{\cos\theta}\right) = \frac{F}{4kl}. \tag{2.3}$$

The solutions θ_{01} and θ_{02} of (2.3) are the static equilibrium values. With $F = 0$, (2.3) shows that the linkage has three equilibrium solutions, namely, $\theta = 0$, $\theta = \theta_0$, and $\theta = -\theta_0$.

The static equilibria can also be obtained using energy methods. The potential energy associated with the system, which is the difference between the potential energy stored in the spring and the work done by the external force, is given by

$$P \triangleq 2kl^2(\cos\theta - \cos\theta_0)^2 - Fl(\sin\theta_0 - \sin\theta). \tag{2.4}$$

Then the static equilibria of the system are given by

$$\frac{\partial P}{\partial\theta} = 0,$$

which yields

$$(\sin\theta)\left(1 - \frac{\cos\theta_0}{\cos\theta}\right) = \frac{F}{4kl}, \tag{2.5}$$

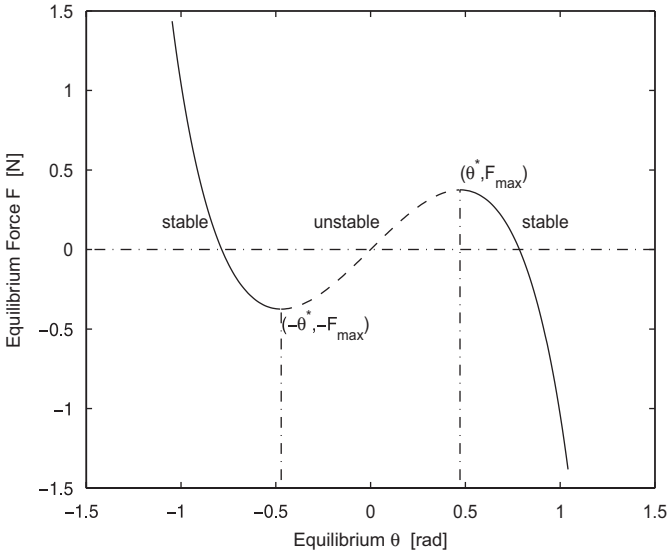

Fig. 5. Dependence of the static equilibrium force F on θ given by (2.5). Chosen parameter values are $\theta_0 = \frac{\pi}{4}$ rad, $k = 1$ N m, and $l = 1$ m. For the given parameters, $\theta^* = -0.4715$ rad and $F_{\max} = 0.3747$ N.

which is the same as (2.3). Fig. 5 shows F as a function of θ. Let $F_{\max}$ be the local maximum value of F and let $\theta = \theta^*$ at $F = F_{\max}$. Solving $\frac{dF}{d\theta} = 0$, where F is given by (2.5), yields

$$\theta^* = \cos^{-1}((\cos\theta_0)^{1/3}). \tag{2.6}$$

To analyze the stability of the static equilibria, we evaluate the second derivative of the potential energy P, which is given by

$$\frac{1}{4kl^2}\frac{\partial^2 P}{\partial\theta^2} = -(\cos\theta)(\cos\theta - \cos\theta_0) + \sin^2\theta - \frac{F}{4kl}\sin\theta. \tag{2.7}$$

Substituting (2.5) into (2.7) yields

$$\frac{1}{4kl^2}\frac{\partial^2 P}{\partial\theta^2} = -(\cos\theta)(\cos\theta - \cos\theta_0) + \sin^2\theta - (\sin^2\theta)\left(1 - \frac{\cos\theta_0}{\cos\theta}\right),$$

which can be rewritten as

$$\frac{1}{4kl^2}\frac{\partial^2 P}{\partial\theta^2} = (\cos\theta_0 - \cos^3\theta)\frac{1}{\cos\theta}. \tag{2.8}$$

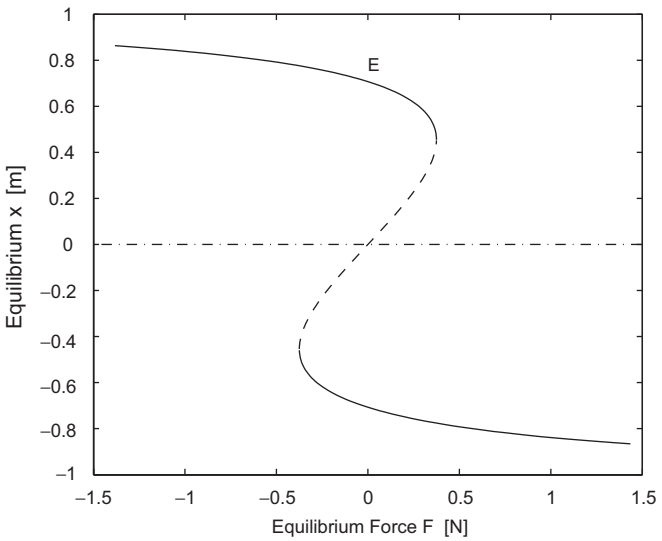

Fig. 6. Equilibrium set $\mathscr{E}$ for the preloaded two-bar linkage. The chosen parameter values are $\theta_0 = \pi/4$ rad, $k = 1$ N m, and $l = 1$ m.

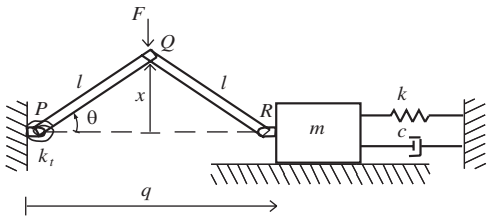

Fig. 7. The two-bar linkage model with a torsional spring k_t.

Using the potential energy theorem [27, p. 56], the condition $\frac{\partial^2 P}{\partial \theta^2} > 0$ implies that the equilibrium θ is stable for $\theta < -\theta^*$ and $\theta > \theta^*$, whereas $\frac{\partial^2 P}{\partial \theta^2} < 0$ implies that the equilibrium θ is unstable for $-\theta^* < \theta < \theta^*$.

Definition 2.1. The *equilibrium set* $\mathscr{E}$ for the preloaded two-bar linkage is the set of points (F, x) that satisfy

$$x\left(1 - \frac{l\cos\theta_0}{\sqrt{l^2 - x^2}}\right) = \frac{F}{4k}. \tag{2.9}$$

Note that x is the vertical distance from the joint Q to the horizontal equilibrium as shown in Fig. 1, while the relation (2.9) is obtained from (2.5) using $x = l\sin\theta$. The equilibrium set $\mathscr{E}$ shown in Fig. 6 is useful for analyzing the hysteresis of the preloaded two-bar linkage, as shown in Section 6.

Now, consider the preloaded two-bar linkage with a torsional spring $k_t > 0$ as shown in Fig. 7. To find the static equilibria for this system, we set the net torque about joint P to zero, which yields

$$Fl\cos\theta + k_t\theta = C_1 l\sin(2\theta).$$

Using (2.2) and substituting $q = 2l\cos\theta$, we obtain

$$Fl\cos\theta + k_t\theta = 4kl^2(\cos\theta - \cos\theta_0)\sin\theta. \tag{2.10}$$

Assuming $F = 0$, the static equilibria satisfy

$$k_t\theta = 4kl^2(\cos\theta - \cos\theta_0)\sin\theta. \tag{2.11}$$

Eq. (2.11) is satisfied by $\theta = 0$ as well as all θ satisfying

$$\cos\theta = \frac{k_t}{4kl^2} + \cos\theta_0. \tag{2.12}$$

Note that (2.12) has a non-zero solution θ if and only if $0 \leqslant k_t \leqslant 4kl^2(1 - \cos\theta_0)$. Furthermore, if $k_t \geqslant 4kl^2(1 - \cos\theta_0)$, then the preloaded two-bar linkage has exactly one equilibrium, namely, $\theta = 0$.

3. Dynamics of the preloaded two-bar linkage

We now derive the equations of motion for the preloaded two-bar linkage. The system has one degree of freedom given by the angle θ, which can be viewed as the joint-space variable. Let m_{bar} be the inertia of each bar. Ignoring gravity, the kinetic and potential energies of the system are given by

$$T = \tfrac{1}{2}m\dot{q}^2 + T_{\text{bars}}, \quad V = \tfrac{1}{2}k(q - q_0)^2,$$

where T_{bars} is the kinetic energy of the bars. Substituting $q = 2l\cos\theta$ and $T_{\text{bars}} = (\frac{9}{8}m_{\text{bar}}l^2\sin^2\theta + \frac{5}{24}m_{\text{bar}}l^2)\dot{\theta}^2$ we obtain

$$T = ((2ml^2 + \tfrac{9}{8}m_{\text{bar}}l^2)\sin^2\theta + \tfrac{5}{24}m_{\text{bar}}l^2)\dot{\theta}^2, \tag{3.1}$$

$$V = 2kl^2(\cos\theta - \cos\theta_0)^2. \tag{3.2}$$

The generalized non-conservative force Q_{nc} is given by

$$Q_{\text{nc}} = -Fl\cos\theta - 4cl^2\dot{\theta}\sin^2\theta. \tag{3.3}$$

Now, Lagrange's equation $\frac{d}{dt}(\frac{\partial L}{\partial \dot{\theta}}) - \frac{\partial L}{\partial \theta} = Q_{\text{nc}}$, where $L = T - V$, yields

$$\begin{aligned}&\left(\left(2ml^2 + \frac{9}{8}m_{\text{bar}}l^2\right)\sin^2\theta + \frac{5}{24}m_{\text{bar}}l^2\right)\ddot{\theta}\\ &\quad + \left(2ml^2 + \frac{9}{8}m_{\text{bar}}l^2\right)(\sin\theta)(\cos\theta)\dot{\theta}^2\\ &\quad + 2cl^2(\sin^2\theta)\dot{\theta} + 2kl^2(\cos\theta_0 - \cos\theta)(\sin\theta) = -\frac{l\cos\theta}{2}F.\end{aligned} \tag{3.4}$$

Note that, if $m_{\text{bar}} > 0$, then (3.4) has non-singular inertia for all values of θ. However, if $m_{\text{bar}} = 0$, then (3.4) has an inertia singularity for $\theta = 0$.

Next, note that the transformation

$$q = 2l\cos\theta \tag{3.5}$$

is invertible for all $\theta \in (-\frac{\pi}{2}, \frac{\pi}{2})$. However, the velocity relation

$$\dot{q} = -2l(\sin\theta)\dot{\theta} \tag{3.6}$$

is singular for $\theta = 0$. Using $q = 2l\cos\theta$ the dynamics (3.4) can be expressed in terms of the displacement q (that is, the

task-space variable) as

$$((m+\tfrac{9}{16}m_{\text{bar}})(4l^2-q^2)+\tfrac{5}{12}m_{\text{bar}}l^2)(4l^2-q^2)\ddot{q} + \tfrac{5}{12}m_{\text{bar}}l^2q\dot{q}^2+c\dot{q}(4l^2-q^2)^2 + k(q-q_0)(4l^2-q^2)^2=\tfrac{1}{2}q(4l^2-q^2)^{3/2}F. \quad (3.7)$$

Note that (3.7) has an inertia singularity at $q=2l$, that is, for $\theta=0$, whether or not $m_{\text{bar}}=0$. Note also that if $m_{\text{bar}}\neq 0$ and $q=2l$, then $\dot{q}=0$, that is, the mass m always come to rest when the links are horizontal.

4. Linearization

Throughout the section we assume that $m_{\text{bar}}=0$. For this case, the dynamics (3.4) become

$$2ml^2(\sin^2\theta)\ddot{\theta}+2ml^2(\sin\theta)(\cos\theta)\dot{\theta}^2+2cl^2(\sin^2\theta)\dot{\theta} + 2kl^2(\cos\theta_0-\cos\theta)(\sin\theta)=-\frac{l\cos\theta}{2}F. \quad (4.1)$$

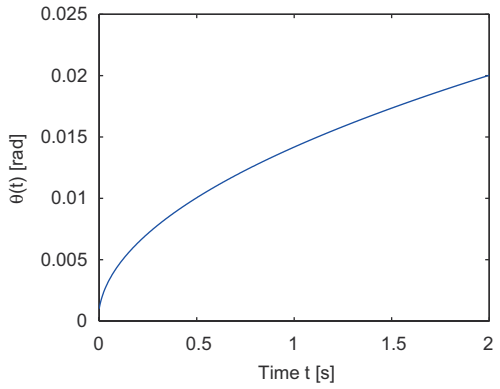

Fig. 8. Trajectory of the angle θ evaluated using (4.9) for the initial condition $\theta(0)=0.001$ rad and $\dot{\theta}(0)=0.1$ rad/s. Note that the instability is sublinear and thus non-polynomial and non-exponential, in accordance with the fact that the dynamics are not linearizable at the unstable equilibrium.

Defining $x_1=\theta$ and $x_2=\dot{\theta}$, (4.1) can be written as

$$\begin{bmatrix}\dot{x}_1\\ \dot{x}_2\end{bmatrix}=\begin{bmatrix}x_2\\ -\dfrac{\cos x_1}{\sin x_1}x_2^2-\dfrac{c}{m}x_2-\dfrac{k}{m}\dfrac{\cos\theta_0-\cos x_1}{\sin x_1}\end{bmatrix} - \begin{bmatrix}0\\ \dfrac{\cos x_1}{4ml\sin^2 x_1}\end{bmatrix}F. \quad (4.2)$$

To linearize (4.2), we evaluate the Jacobian as

$$J=\begin{bmatrix}0 & 1\\ \dfrac{x_2^2}{\sin^2 x_1}+\dfrac{k\cos\theta_0}{(\sin x_1)(\cos x_1)} & \dfrac{-2x_2^2}{\tan x_1}-\dfrac{c}{m}\end{bmatrix}. \quad (4.3)$$

However, J does not exist at $x_1=0$, $x_2=0$, and thus the system does not have a linearization at the horizontal equilibrium.

Alternatively, to analyze the behavior near the horizontal equilibrium, we substitute the small-angle approximations $\sin\theta\cong\theta$ and $\cos\theta\cong 1$ in (4.1) to obtain

$$m\theta^2\ddot{\theta}+m\theta\dot{\theta}^2+c\theta^2\dot{\theta}-k\theta(1-\cos\theta_0)=-\frac{F}{4l}. \quad (4.4)$$

Now assume $F=0$. Then, for non-zero θ, (4.4) can be rewritten as

$$\theta\ddot{\theta}+\dot{\theta}^2+\frac{c}{m}\theta\dot{\theta}-\alpha=0, \quad (4.5)$$

where $\alpha\triangleq\frac{k}{m}(1-\cos\theta_0)$ is a positive constant. Using $\theta\ddot{\theta}+\dot{\theta}^2=\frac{\mathrm{d}}{\mathrm{d}t}(\theta\dot{\theta})$, (4.5) can be written as

$$\frac{\mathrm{d}}{\mathrm{d}t}(\theta\dot{\theta})+\frac{c}{m}\theta\dot{\theta}=\alpha. \quad (4.6)$$

The solution to the first-order differential equation (4.6) is then

$$\theta\dot{\theta}=\beta\mathrm{e}^{-c/mt}+\frac{\alpha m}{c}, \quad (4.7)$$

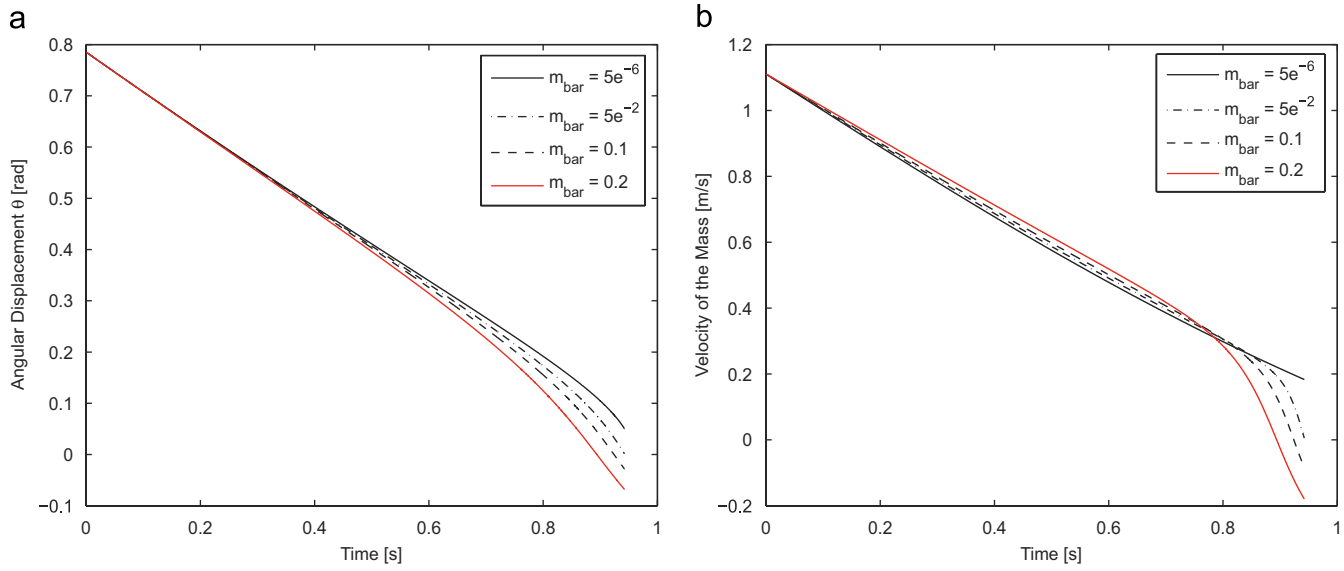

Fig. 9. Time histories of θ and the velocity $\dot{q}$ of the mass for various values of m_{bar} with initial conditions $q(0)=\sqrt{2}$ m and $\dot{q}(0)=1.1$ m/s. The velocity $\dot{q}$ of the mass reaches zero increasingly abruptly as m_{bar} decreases. The parameter values used are $k=1$ N/m, $m=1$ kg, $l=1$ m, and $q_0=\sqrt{2}$ m.

where $\beta \triangleq \theta(0)\dot{\theta}(0) - \frac{\alpha m}{c}$. Integrating (4.7) yields

$$\theta(t) = \left[\theta^2(0) - 2\frac{\beta m}{c}(e^{-c/mt} - 1) + 2\frac{\alpha m}{c}t\right]^{1/2}. \tag{4.8}$$

Eq. (4.8) can be approximated for small $t > 0$ as

$$\theta(t) \approx \left[\theta^2(0) + 2\left(\beta + \frac{\alpha m}{c}\right)t\right]^{1/2}. \tag{4.9}$$

Note that the approximate solution (4.9) does not correspond to the solution of a linear system, which is consistent with the fact that the linkage is not linearizable at the horizontal equilibrium. The trajectory of the angle θ evaluated using (4.9) with the initial condition $\theta(0) = 0.001$ rad and $\dot{\theta}(0) = 0.1$ rad/s is shown in Fig. 8.

We now consider the motion of the mass m as $\theta \to 0$. Fig. 9 shows time histories of θ and $\dot{q}$ for various values of m_{bar}. Note that as m_{bar} decreases, the velocity $\dot{q}$ of the mass drops to zero increasingly abruptly as $\theta \to 0$. We study this phenomenon in the next section.

5. Analysis of the unstable equilibrium of the undamped preloaded two-bar linkage with inertialess bars

Under the approximating assumption that the bars are inertialess ($m_{\text{bar}} = 0$) and the linkage is undamped ($c = 0$), the free response of the inertialess preloaded two-bar linkage model is given by

$$m(4l^2 - q^2)^2\ddot{q} + k(q - q_0)(4l^2 - q^2)^2 = 0. \tag{5.1}$$

The trajectories of the angle θ and the velocity $\dot{q}$ of the mass obtained by simulating the dynamics in (5.1) with initial conditions $q(0) = \sqrt{2}$ m and $\dot{q}(0) = 1.1$ m/s are shown in Fig. 10.

Fig. 9(b) shows that the velocity $\dot{q}$ of the mass approaches a non-zero value as θ approaches zero and drops discontinuously to zero when $\theta = 0$. The limiting value of $\dot{q}$ can be evaluated using energy conservation. The total energy of the system is

$$E \triangleq \tfrac{1}{2}m\dot{q}^2 + \tfrac{1}{2}k(q - q_0)^2. \tag{5.2}$$

Letting $\dot{q}_\infty$ denote the limiting value of the velocity of the mass as $\theta \to 0$, it follows that

$$\dot{q}_\infty^2 = \dot{q}^2(0) - \frac{k}{m}[(2l - q_0)^2 - (q(0) - q_0)^2]. \tag{5.3}$$

With the initial conditions $q(0) = \sqrt{2}$ m and $\dot{q}(0) = 1.1$ m/s, we obtain $\dot{q}_\infty = 0.94$ m/s, which matches the value obtained numerically in Fig. 10(b) with the parameter values $k = 1$ N/m, $m = 1$ kg, $l = 1$ m, and $q_0 = \sqrt{2}$ m. When $\theta = 0$, we have $q = 2l$, and $\dot{q}$ abruptly drops to zero. The velocity $\dot{q} = 0$ at $\theta = 0$ is consistent with the kinematic relation (3.6). Fig. 9(b) shows that the discontinuity in $\dot{q}$ disappears when m_{bar} is positive.

As $\theta \to 0$, the magnitude of the angular velocity of the bars increases rapidly as shown in Fig. 11(b). Since the bars are assumed to be inertialess, their behavior at $\theta = 0$ cannot be predicted using energy conservation or Newton's laws. This unpredictability indicates that the dynamics (5.1) can possess non-unique solutions.

To investigate the existence of non-unique solutions, we consider the initial state

$$q(0) = 2l, \quad \dot{q}(0) = 0, \tag{5.4}$$

at which the total energy of the system is

$$E_0 \triangleq \tfrac{1}{2}k(2l - q_0)^2.$$

By conservation of energy, $E = E_0$ yields

$$\dot{q}^2 = \frac{k}{m}[(2l - q_0)^2 - (q - q_0)^2], \tag{5.5}$$

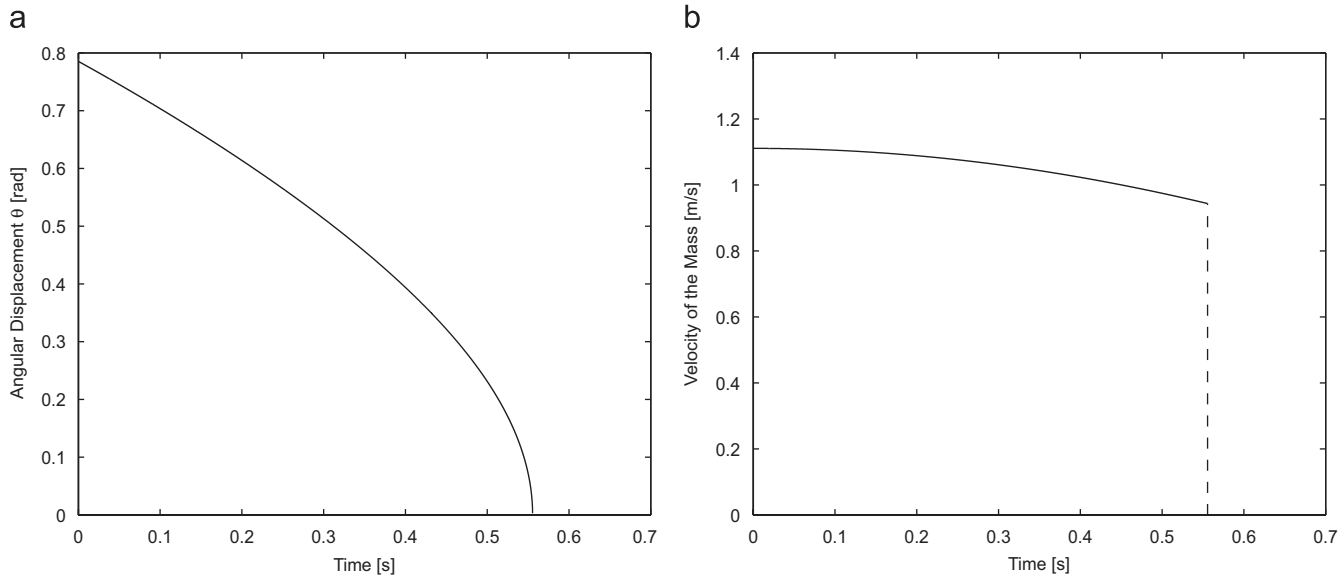

Fig. 10. Time histories of θ and the velocity $\dot{q}$ of the mass with initial conditions $q(0) = \sqrt{2}$ m and $\dot{q}(0) = 1.1$ m/s. These plots show that $\dot{q} \to 0.94$ m/s as $\theta \to 0$ rad. However, $\dot{q}$ discontinuously drops to zero when $\theta = 0$ rad. The parameter values used are $k = 1$ N/m, $m = 1$ kg, $m_{\text{bar}} = 0$ kg, $l = 1$ m, and $q_0 = \sqrt{2}$ m.

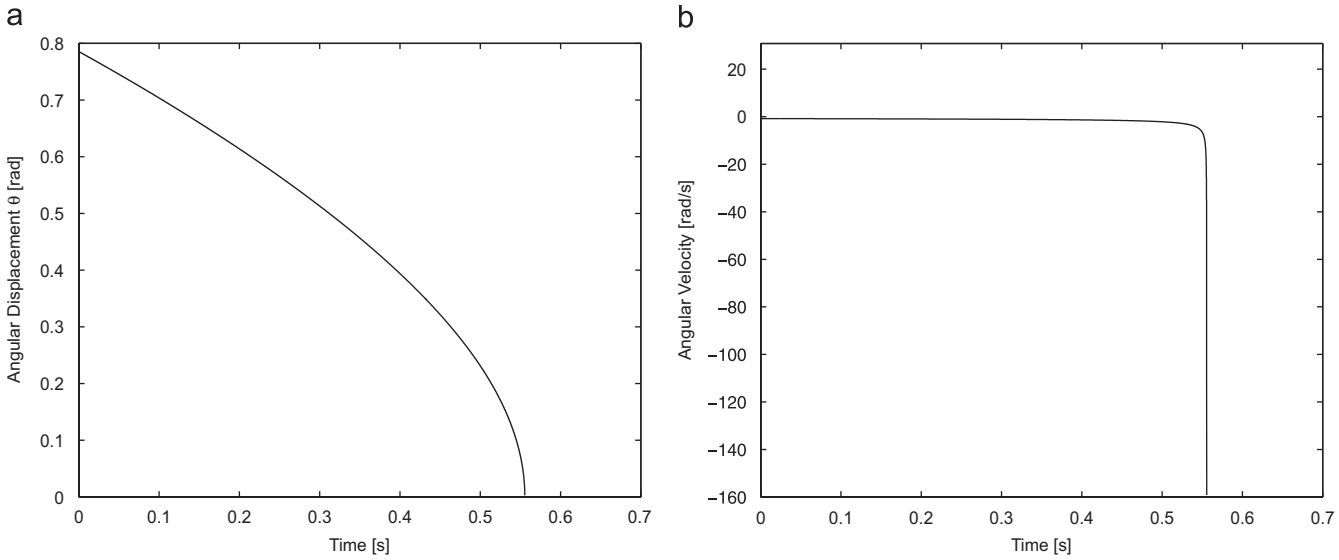

Fig. 11. Time histories of θ and $\dot{\theta}$ with initial conditions $q(0)=\sqrt{2}\,\mathrm{m}$ and $\dot{q}(0)=1.1\,\mathrm{m/s}$. The magnitude of the angular velocity of the bars increases rapidly as $\theta \to 0$. The parameter values used are as in Fig. 10.

which describes the motion of the undamped system starting at the unstable equilibrium (5.4).

Next, (5.5) can be rewritten as

$$\dot{q} = \sqrt{\frac{k}{m}}\sqrt{[(2l-q_0)^2-(q-q_0)^2]}. \tag{5.6}$$

The expression for $\dot{q}$ in (5.6) is non-Lipschitzian at $q=2l$, thus indicating the possible existence of multiple solutions. Integrating (5.6) we obtain

$$q(t) = q_0 + (2l-q_0)\sin\left(\frac{\pi}{2}+\sqrt{k/m}t\right). \tag{5.7}$$

Direct substitution of (5.7) in (5.1) confirms that $q(t)$ given by (5.7) satisfies (5.1) with the initial conditions (5.4). Note that $q(t)$ given by (5.7) is C^∞, that is, infinitely differentiable.

Next, define the delayed function

$$\begin{aligned} q_T(t) &= 2l, \quad t \leqslant T, \\ &= q(t-T), \quad t > T. \end{aligned} \tag{5.8}$$

The function $q_T(t)$ corresponds to the linkage remaining at the horizontal equilibrium until time T and then spontaneously moving away as shown in Fig. 12. It follows by direct substitution that, for all $T \geqslant 0$, the function $q_T(t)$ satisfies (5.1) with the initial conditions (5.4). Hence, (5.1) has an infinite number of solutions (parameterized by T) that satisfy the initial conditions (5.4). Note that the function $q_T(t)$ is C^1 since $\lim_{t\to T^+}\dot{q}_T(t) = \lim_{t\to T^-}\dot{q}_T(t)=0$. However, for $T>0$, $q_T(t)$ is not C^2 since $\lim_{t\to T^-}\ddot{q}_T(t)=0$ and $\lim_{t\to T^+}\ddot{q}_T(t)=(q_0-2l)\,k/m$. An example of dynamics that exhibit analogous non-unique solutions is given in [28]. Due to the singularity in (5.1) at $q=2l$, it is also possible for the links to arrive with zero velocity at the horizontal equilibrium, which is unstable.

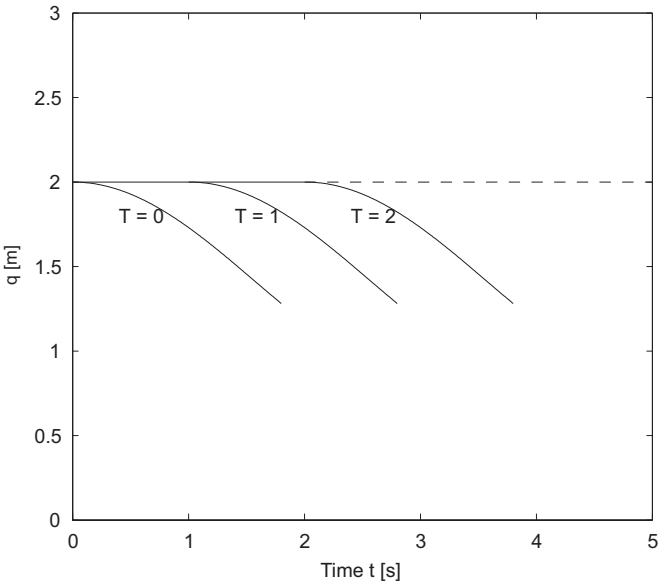

Fig. 12. Non-unique solutions of the undamped preloaded two-bar linkage dynamics with inertialess bars given by (5.8) for various values of T. The parameters used are $k=1\,\mathrm{N/m}$, $m=1\,\mathrm{kg}$, $m_{\mathrm{bar}}=0\,\mathrm{kg}$, $l=1\,\mathrm{m}$, and $q_0=2l\cos(\frac{\pi}{4})\,\mathrm{m}$.

6. Hysteresis in the preloaded two-bar linkage

The hysteresis map of a system is the response of the system in the limit of DC operation, that is, the response under periodic inputs with frequency approaching zero [3,5]. Hence, the hysteresis map of a system is closely related to the equilibrium set $\mathscr{E}$, which is the set of constant input and output pairs corresponding to static equilibria of the system. It is shown in [29] that a system that exhibits hysteresis has a multi-valued equilibrium map and that the hysteresis map is a subset of the equilibrium map. It can be seen from the equilibrium set $\mathscr{E}$ in Fig. 6 that multiple equilibria exist for each constant $F \in (-F_{\max}, F_{\max})$.

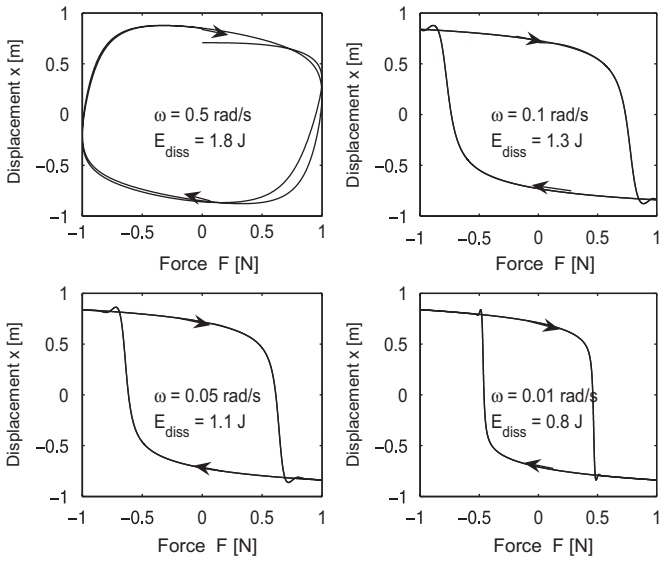

Fig. 13. Input–output maps between the vertical force F and the vertical displacement x for the two-bar linkage model (3.4) for several values of frequency ω in rad/s. The non-vanishing clockwise displacement-force loop at asymptotically low frequencies is the hysteresis map. E_{diss}, which is the area of each loop, is the energy dissipated by the dashpot in one complete cycle. The parameters used are $k=1\,\text{N/m}$, $m=1\,\text{kg}$, $c=1\,\text{N s/m}$, $m_{\text{bar}}=0.5\,\text{kg}$, $l=1\,\text{m}$, and $F(t)=\sin(\omega t)\,\text{N}$.

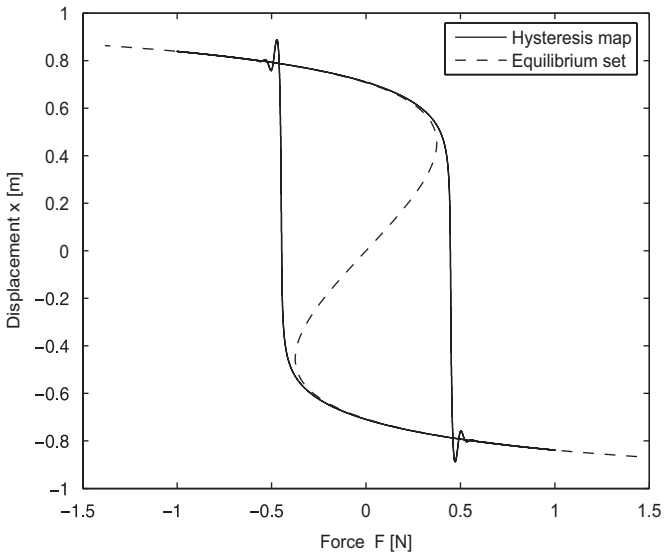

Fig. 14. Comparison of the equilibrium set $\mathscr{E}$ and the hysteresis map for the preloaded two-bar linkage. The hysteresis map is a subset of $\mathscr{E}$ except for the vertical segments at the bifurcation points. The parameters used are as in Fig. 13 with $F(t)=\sin(0.01t)\,\text{N}$.

The existence of multiple equilibria suggests that the system may be hysteretic. We simulate the linkage dynamics given by (3.4) under the periodic external force $F=\sin(\omega t)$ N using the parameter values $k=1\,\text{N/m}$, $m=1\,\text{kg}$, $c=1\,\text{N s/m}$, $m_{\text{bar}}=0.5\,\text{kg}$, and $l=1\,\text{m}$. As shown in Fig. 13 there exists a non-trivial clockwise hysteresis map from the vertical force F to the vertical displacement x (equivalent to a counterclockwise map from the vertical displacement x to the vertical force F) at low frequencies. The vertical displacement is $x=l\sin\theta$. The presence of a non-trivial loop at asymptotically low frequencies constitutes hysteresis. For details see [5]. A comparison of the hysteresis map and the equilibrium set $\mathscr{E}$ for the preloaded two-bar linkage is shown in Fig. 14.

7. Feedback linearization control of the two-bar linkage

The linkage dynamic model (4.1) has an unstable equilibrium at $\theta=0$ leading to snap-through behavior. What makes the model challenging to stabilize is that it does not have a linearization at $\theta=0$, which in turn is due to the presence of $\sin\theta$ in the coefficients of $\ddot{\theta}$ and $\dot{\theta}$.

To stabilize the linkage at $\theta=0$, we use feedback linearization to generate a control signal that makes θ decay according to the second-order system

$$\ddot{\theta}=-a\dot{\theta}-b\theta, \tag{7.1}$$

where $a>0$ and $b>0$. Substituting (7.1) into (4.1) we obtain

$$m[(\sin^2\theta)(-a\dot{\theta}-b\theta)+(\sin\theta)(\cos\theta)\dot{\theta}^2] + c(\sin^2\theta)\dot{\theta}+k(\sin\theta)(\cos\theta_0-\cos\theta)=-\frac{\cos\theta}{4l}F.$$

Solving for F yields

$$F=-\frac{4l}{\cos\theta}[m(\sin\theta)(\cos\theta)\dot{\theta}^2-(ma-c)(\sin^2\theta)\dot{\theta} - mb(\sin^2\theta)\theta+k(\sin\theta)(\cos\theta_0-\cos\theta)]. \tag{7.2}$$

To illustrate (7.2) we choose the parameter values $a=1\,\text{s}^{-1}$, $b=1\,\text{s}^{-2}$, $m=1\,\text{kg}$, $c=1\,\text{N s/m}$, $k=1\,\text{N/m}$, $l=1\,\text{m}$, and $\theta_0=\frac{\pi}{4}$ rad. For the initial conditions $\theta(0)=\frac{\pi}{4}$ rad and $\dot{\theta}(0)=1\,\text{rad/s}$, the time histories of θ, $\dot{\theta}$, and the control input F are shown in Figs. 15 and 16, respectively. Similarly, for the initial conditions $\theta(0)=-\frac{\pi}{3}$ rad and $\dot{\theta}(0)=1.5\,\text{rad/s}$, the time histories of θ, $\dot{\theta}$, and the control input F are shown in Figs. 17 and 18, respectively.

8. Intrinsic non-linear proportional-derivative control

Since the feedback-linearization controller in Section 7 requires knowledge of all of the linkage parameters, we now develop an intrinsic non-linear proportional-derivative (INPD) controller based on the theory given in [25,30]. In [25], a robust non-linear controller is given for fully actuated mechanical systems. Since the two-bar linkage is fully actuated, the theory given in [25,30] is applicable.

The control law given in [25] requires the construction of an error function as well as design functions Φ and Ψ [30]. First, note that the configuration space of the preloaded two-bar linkage has the topology of S^1. Let $\theta\in[-\pi,\pi)$ parameterize S^1, and let $\theta_s\in[-\pi,\pi)$ denote the desired setpoint. Then, one choice [30] of an error function $e: S^1\to\mathbb{R}$ is given by $e(\theta)=1-\cos(\theta_s-\theta)$.

To stabilize $\theta_s=0$, the error function is given by $e(\theta)=1-\cos\theta$, and we choose $\Phi(\theta)=k_1 l\theta$ and $\Psi(\theta,\dot{\theta})=k_2 l\dot{\theta}$, where

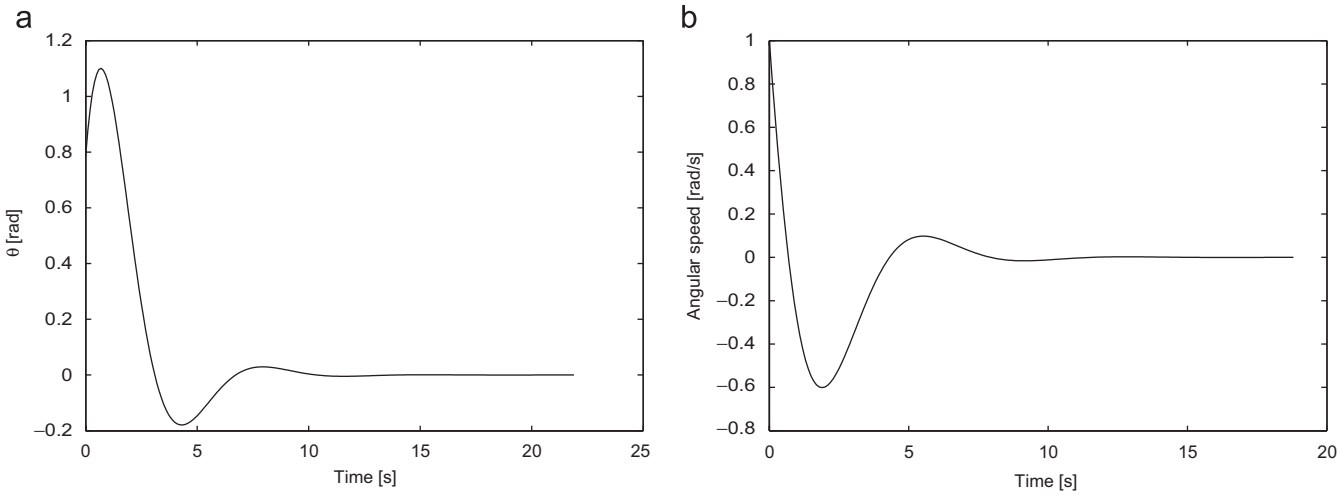

Fig. 15. Time histories of θ and $\dot{\theta}$ under the action of the feedback linearization controller (7.2) with initial conditions $\theta(0) = \frac{\pi}{4}$ rad and $\dot{\theta}(0) = 1$ rad/s. The controller stabilizes the horizontal equilibrium.

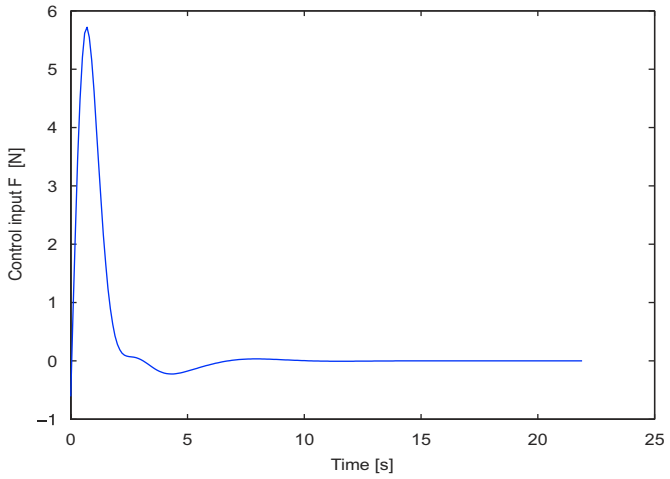

Fig. 16. Control input F given by (7.2) with initial conditions $\theta(0) = \frac{\pi}{4}$ rad and $\dot{\theta}(0) = 1$ rad/s.

$k_1, k_2 > 0$. Then, the control law in [25] for the preloaded two-bar linkage is given by

$$F = -\frac{1}{\cos\theta}u, \tag{8.1}$$

where

$$u = -\frac{\Phi'(e(\theta))}{l}\frac{\partial e}{\partial\theta}(\theta) + \frac{1}{l}\frac{\partial V}{\partial\theta}(\theta) - \frac{\Psi(\theta,\dot{\theta})}{l} + \frac{u_f}{l}, \tag{8.2}$$

$V \triangleq 2kl^2(\cos\theta - \cos\theta_0)^2$ is the potential energy, and $u_f \triangleq 4cl^2\sin^2(\theta)\dot{\theta}$ is the energy dissipated by the damping force. Using (8.2), we obtain the INPD controller

$$u = -[k_1 + 4kl(\cos\theta - \cos\theta_0)]\sin\theta - (k_2 - 4cl\sin^2\theta). \tag{8.3}$$

The controller (8.3) asymptotically stabilizes the desired equilibrium with local exponential convergence such that its domain of attraction contains a compact sublevel set of a Lyapunov function [25,30]. Since (8.3) does not require knowledge of the mass m or the linkage mass m_{bar}, this control law is unconditionally robust with respect to the inertia parameters of the system.

Although the INPD controller (8.3) is unconditionally robust with respect to inertia parameters, it requires complete knowledge of the potential function $V(\theta)$ given in (3.2). We now remove this limitation by presenting a robust version of the INPD controller, which requires less modeling information than the INPD controller (8.3).

Theorem 8.1. *Consider the two-bar linkage model* (3.4), *and choose F as in* (8.1) *and*

$$u = -k_p\sin\theta - k_d\dot{\theta}, \tag{8.4}$$

where $k_p > 4kl$ and $k_d \geqslant 0$. Then the function $\mathscr{V} : S^1 \times \mathbb{R} \to \mathbb{R}$ given by

$$\mathscr{V}(\theta,\dot{\theta}) \triangleq \left(\left(2ml^2 + \frac{9}{8}m_{\text{bar}}l^2\right)\sin^2\theta + \frac{5}{24}m_{\text{bar}}l^2\right)\dot{\theta}^2 + kl^2\left[\left(\frac{k_p}{kl} - 2\right) + 2(2\cos\theta_0 - \cos\theta)\right] \times (1 - \cos\theta) \tag{8.5}$$

is a Lyapunov function for (4.1), (8.1), (8.4) *such that the equilibrium $(\theta,\dot{\theta}) = (0,0)$ is asymptotically stable with a domain of attraction that contains a sublevel set of $\mathscr{V}$. Furthermore, the set $\{(\theta,\dot{\theta}) \in (-\pi/2,\pi/2)\times\mathbb{R} : \dot{\theta} = 0\}$ is contained in the domain of attraction, and $(\theta,\dot{\theta}) = (0,0)$ is the only asymptotically stable equilibrium of* (4.1), (8.1), (8.4). *Finally, if $k_d > 0$, then the closed-loop solutions converge to the equilibrium $(\theta,\dot{\theta}) = (0,0)$ locally exponentially fast.*

Proof. Consider the closed-loop system formed by the two-bar linkage model (3.4), where F satisfies (8.1) and u is given by (8.4).

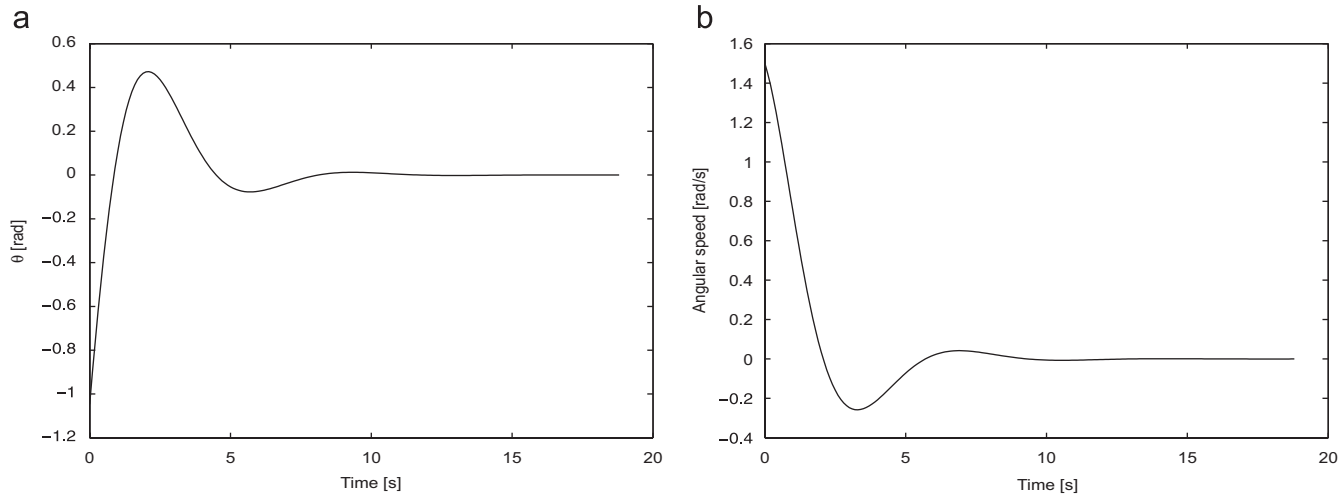

Fig. 17. Time histories of θ and $\dot{\theta}$ under the action of the non-linear controller (7.2) with initial conditions $\theta(0) = -\frac{\pi}{3}$ rad and $\dot{\theta}(0) = 1.5$ rad/s. The controller stabilizes the horizontal equilibrium. The parameter values used are $a = 1\,\mathrm{s}^{-1}$, $b = 1\,\mathrm{s}^{-2}$, $m = 1$ kg, $c = 1$ N s/m, $k = 1$ N/m, $l = 1$ m, and $\theta_0 = \frac{\pi}{4}$ rad.

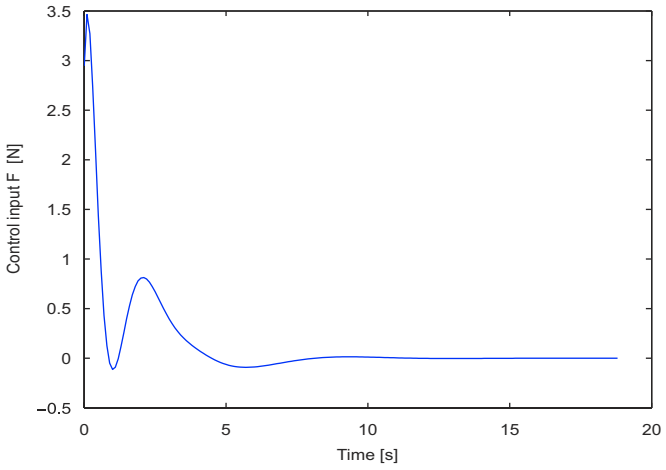

Fig. 18. Control input F given by (7.2) with initial conditions $\theta(0) = -\frac{\pi}{3}$ rad and $\dot{\theta}(0) = 1.5$ rad/s. The parameter values used are same as in Fig. 17.

To show that $\mathscr{V}$ is positive definite on $S^1 \times \mathbb{R}$, note that the first term in (8.5) is non-negative. Consider the second term in (8.5). A plot of this term for various values of θ_0 is shown in Fig. 19. Since $k_p > 4kl$ and $\theta_0 \in [0, \pi/2]$ it follows that

$$\begin{aligned} & kl^2\left[\left(\frac{k_p}{kl} - 2\right) + 2(2\cos\theta_0 - \cos\theta)\right](1 - \cos\theta) \\ & \geqslant kl^2\left[\frac{k_p}{kl} - 2 - 2\cos\theta\right](1 - \cos\theta) \\ & \geqslant kl^2\left[\frac{k_p}{kl} - 4\right](1 - \cos\theta) \\ & \geqslant kl^2(1 - \cos\theta) \\ & \geqslant 0. \end{aligned}$$

Thus, $\mathscr{V}(\theta, \dot{\theta})$ in (8.5) is non-negative.

Next, equate the RHS of (8.5) to zero. Since both terms in (8.5) are non-negative, both must be equal to zero. The first term yields $\dot{\theta} = 0$. Since the second term is greater than or equal to $kl^2(1 - \cos\theta)$, the second term yields $\theta = 2n\pi$, where $n \in \{0, \pm 1, \pm 2, \ldots\}$. As $\theta \in [-\pi, \pi)$, $\mathscr{V}(\theta, \dot{\theta})$ is zero only at $(\theta, \dot{\theta}) = (0, 0)$. Therefore, $\mathscr{V}(\theta, \dot{\theta})$ is positive definite on $S^1 \times \mathbb{R}$.

Differentiating (8.5) with respect to time along solutions of the closed-loop system yields

$$\begin{aligned} \dot{\mathscr{V}}(\theta, \dot{\theta}) = & 2\left(\left(2ml^2 + \frac{9}{8}m_{\mathrm{bar}}l^2\right)\sin^2\theta + \frac{5}{24}m_{\mathrm{bar}}l^2\right)\dot{\theta}\ddot{\theta} \\ & + \left(4ml^2 + \frac{9}{4}m_{\mathrm{bar}}l^2\right)(\sin\theta)(\cos\theta)\dot{\theta}^3 \\ & + l(k_p - 2kl)(\sin\theta)\dot{\theta} \\ & + 2kl^2(2\cos\theta_0 - \cos\theta)(\sin\theta)\dot{\theta} \\ & + 2kl^2(\sin\theta)(1 - \cos\theta)\dot{\theta} \\ = & 2\dot{\theta}\left\{-2cl^2(\sin^2\theta)\dot{\theta} - 2kl^2(\cos\theta_0 - \cos\theta)\sin\theta \right. \\ & + \frac{lu}{2} + \frac{l}{2}(k_p - 2kl)\sin\theta \\ & \left. + kl^2(2\cos\theta_0 - \cos\theta)\sin\theta + kl^2(\sin\theta)(1 - \cos\theta)\right\} \\ = & 2\dot{\theta}\left\{-2cl^2(\sin^2\theta)\dot{\theta} - 2kl^2(\cos\theta_0 - \cos\theta)\sin\theta \right. \\ & - \frac{l}{2}k_p\sin\theta - \frac{l}{2}k_d\dot{\theta} + \frac{l}{2}k_p\sin\theta - kl^2\sin\theta \\ & \left. + 2kl^2(\cos\theta_0 - \cos\theta)\sin\theta + kl^2\sin\theta\right\} \\ = & -(4cl^2(\sin^2\theta) + k_d)\dot{\theta}^2 \leqslant 0. \end{aligned} \tag{8.6}$$

Thus, $\dot{\mathscr{V}}(\theta, \dot{\theta})$ is negative semidefinite, and hence the equilibrium $(0, 0)$ is Lyapunov stable.

Next, for θ_1 and θ_2 in $[-\pi/2, \pi/2]$, consider the expression

$$\begin{aligned}
&(\mathscr{V}(\theta_1,0)-\mathscr{V}(\theta_2,0))(|\theta_1|-|\theta_2|)\\
&\quad= kl^2\left\{\left[\frac{k_p}{kl}-2+2(2\cos\theta_0-\cos\theta_1)\right](1-\cos\theta_1)\right.\\
&\qquad\left.-\left[\frac{k_p}{kl}-2+2(2\cos\theta_0-\cos\theta_2)\right](1-\cos\theta_2)\right\}\\
&\qquad\times(|\theta_1|-|\theta_2|)\\
&\quad= kl^2(\cos\theta_1-\cos\theta_2)(|\theta_1|-|\theta_2|)\\
&\qquad\times\left[-\frac{k_p}{kl}+2-4\cos\theta_0-2+2(\cos\theta_1+\cos\theta_2)\right]\\
&\quad= kl^2(\cos\theta_1-\cos\theta_2)(|\theta_1|-|\theta_2|)\\
&\qquad\times\left[-\frac{k_p}{kl}-4\cos\theta_0+2(\cos\theta_1+\cos\theta_2)\right]. \qquad (8.7)
\end{aligned}$$

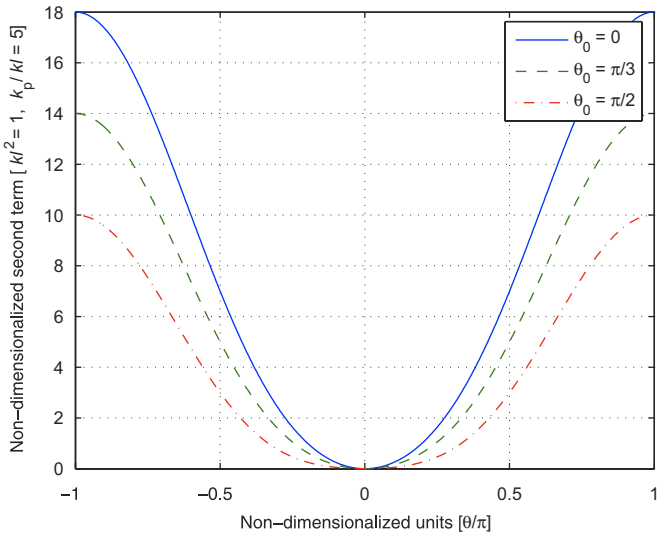

Fig. 19. Plot of the second term in the Lyapunov function (8.5). The plot is for the non-dimensionalized values corresponding to $kl^2 = 1$ and $\frac{k_p}{kl} = 5$.

Since $\theta_0 \in [0, \pi/2]$ and θ_1 and θ_2 lie in $[-\pi/2, \pi/2]$, we have

$$-\frac{k_p}{kl}-4\cos\theta_0+2(\cos\theta_1+\cos\theta_2)\leqslant-\frac{k_p}{kl}+4<0 \qquad (8.8)$$

and, for $\theta_1 \neq \theta_2$,

$$(\cos\theta_1-\cos\theta_2)(|\theta_1|-|\theta_2|)<0. \qquad (8.9)$$

Combining (8.7), (8.8) and (8.9) yields that, if θ_1 and θ_2 lie in $[-\pi/2, \pi/2]$ and $\theta_1 \neq \theta_2$, then $(\mathscr{V}(\theta_1,0)-\mathscr{V}(\theta_2,0))(|\theta_1|-|\theta_2|)>0$. This implies that, for all θ_1 and θ_2 in $[-\pi/2, \pi/2]$, $\mathscr{V}(\theta_1,0)<\mathscr{V}(\theta_2,0)$ if and only if $|\theta_1|<|\theta_2|\leqslant\pi/2$.

Now let $\varepsilon \in (0, \mathscr{V}(\pi/2,0))$ and consider the sublevel set of the Lyapunov function $\mathscr{V}(\theta,\dot\theta)$ given as

$$\mathscr{K}_\varepsilon \triangleq \{(\theta,\dot\theta)\in[-\pi,\pi)\times\mathbb{R}:\mathscr{V}(\theta,\dot\theta)\leqslant\mathscr{V}(\pi/2,0)-\varepsilon\}. \qquad (8.10)$$

Note that, for all $(\theta,\dot\theta)\in\mathscr{K}_\varepsilon$,

$$\mathscr{V}(\theta,0)\leqslant\mathscr{V}(\theta,\dot\theta)<\mathscr{V}(\pi/2,0).$$

Since $\mathscr{V}(\theta_1,0)<\mathscr{V}(\theta_2,0)$ if and only if $|\theta_1|<|\theta_2|\leqslant\pi/2$, it follows that every $(\theta,\dot\theta)\in\mathscr{K}_\varepsilon$ satisfies $|\theta|<\pi/2$. Thus the control law (8.1), where u is given in (8.4), is well-defined for any trajectory in $\mathscr{K}_\varepsilon$.

It is clear that $\mathscr{K}_\varepsilon$ is a compact, invariant sublevel set of the Lyapunov function $\mathscr{V}(\theta,\dot\theta)$ given in (8.5) for every $\varepsilon\in(0,\mathscr{V}(\pi/2,0))$. From the invariant set theorem, the closed-loop solution for an initial condition in $\mathscr{K}_\varepsilon$ converges to the largest invariant set in $\{(\theta,\dot\theta)\in\mathscr{K}_\varepsilon:\dot{\mathscr{V}}(\theta,\dot\theta)=0\}$.

Next, it can easily be shown that the largest invariant set in $\mathscr{K}_\varepsilon$ such that $\dot{\mathscr{V}}(\theta,\dot\theta)=0$ is the equilibrium $(\theta,\dot\theta)=(0,0)$. Thus, the equilibrium $(0,0)$ is asymptotically stable, and the sublevel set $\mathscr{K}_\varepsilon$ is contained in the domain of attraction of the closed-loop equilibrium $(0,0)$ for every $\varepsilon\in(0,\mathscr{V}(\pi/2,0))$.

Let $(\theta_0,0)$ be an arbitrary initial condition in the set $\{(\theta,\dot\theta)\in(-\pi/2,\pi/2)\times\mathbb{R}:\dot\theta=0\}$. Then, since $\mathscr{V}(\theta_1,0)<\mathscr{V}(\theta_2,0)$

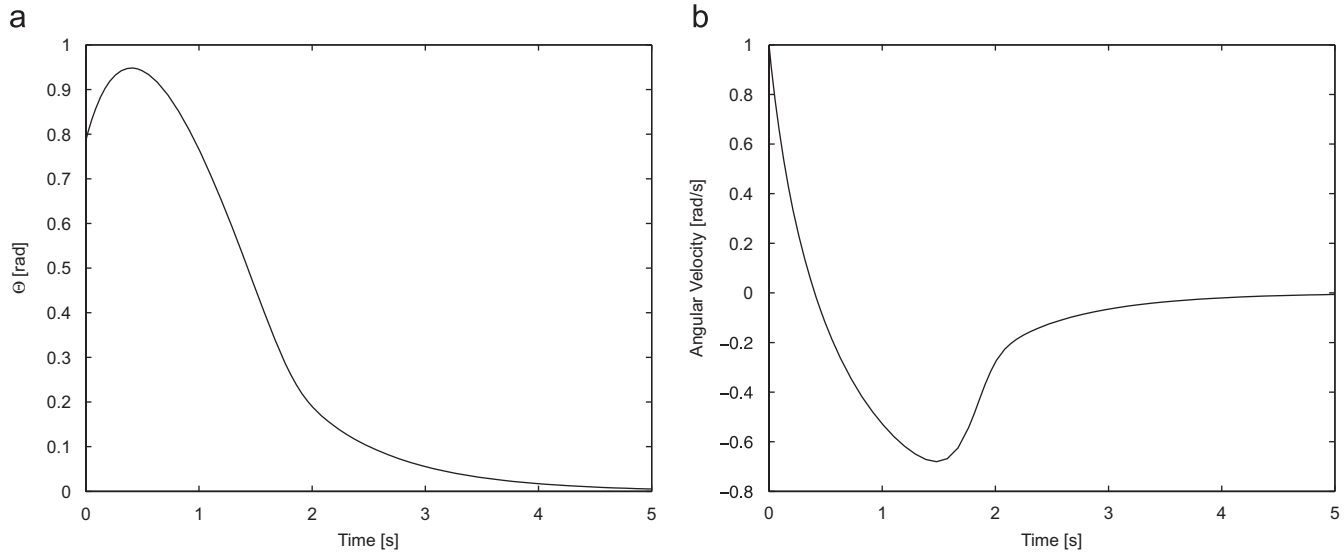

Fig. 20. Time histories of θ and $\dot\theta$ of (4.1) under the action of the non-linear controller (8.1), (8.4) with initial conditions $\theta(0)=\frac{\pi}{4}$ rad and $\dot\theta(0)=1$ rad/s. The controller stabilizes the horizontal equilibrium.

if and only if $|\theta_1| < |\theta_2| \leqslant \pi/2$, it follows that $\mathscr{V}(\theta_0, 0) < \mathscr{V}(\pi/2, 0)$. Therefore, there exists $\varepsilon_0 \in (0, \mathscr{V}(\pi/2, 0))$ such that $\mathscr{V}(\theta_0, 0) \leqslant \mathscr{V}(\pi/2, 0) - \varepsilon_0$. Thus, $(\theta_0, 0) \in \mathscr{K}_{\varepsilon_0}$ and hence $(\theta_0, 0)$ lies in a sublevel set contained in the domain of attraction of the equilibrium $(0, 0)$. Therefore, the set $\{(\theta, \dot{\theta}) \in (-\pi/2, \pi/2) \times \mathbb{R} : \dot{\theta} = 0\}$ lies in the domain of attraction of the equilibrium $(0, 0)$ of the closed-loop system.

Suppose $k_d > 0$. Then linearizing the closed-loop equations (4.1), (8.4), it can be shown that the equilibrium $(0, 0)$ is hyperbolic (see [31]). Since the equilibrium $(0, 0)$ is asymptotically stable, this implies that all eigenvalues of the linearization of the closed-loop lie in the open left half plane. Therefore, the non-linear closed-loop system converges locally exponentially fast to the equilibrium $(0, 0)$.

Next, consider the closed-loop dynamics obtained by substituting (8.4) into (4.1) yielding

$$m[(\sin^2\theta)\ddot{\theta} + (\sin\theta)(\cos\theta)\dot{\theta}^2] + c(\sin^2\theta)\dot{\theta} + k(\sin\theta)(\cos\theta_0 - \cos\theta) = -\frac{\cos\theta}{4l}\frac{k_p \sin\theta + k_d\dot{\theta}}{\cos\theta}.$$

To determine the static equilibria, we set all derivatives to zero, yielding

$$k(\sin\theta)\left(\cos\theta_0 + \frac{k_p}{4kl} - \cos\theta\right) = 0. \tag{8.11}$$

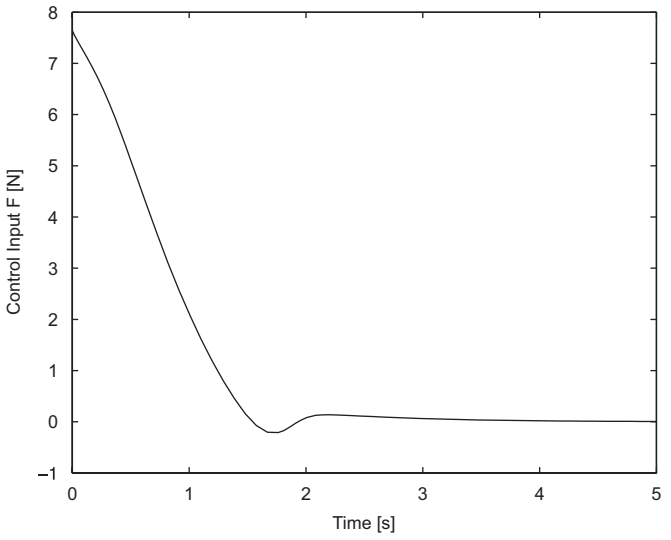

Fig. 21. Control input F given by (8.4) with initial conditions $\theta(0) = \frac{\pi}{4}$ rad and $\dot{\theta}(0) = 1$ rad/s.

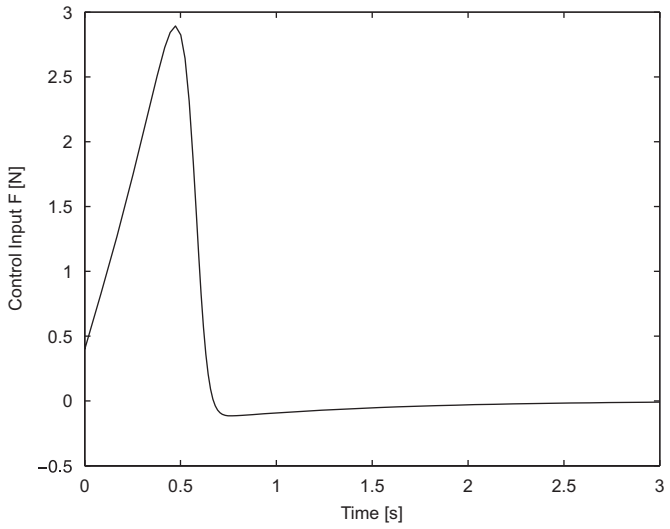

Fig. 23. Control input F given by (8.4) with initial conditions $\theta(0) = -\frac{\pi}{3}$ rad and $\dot{\theta}(0) = -1.5$ rad/s.

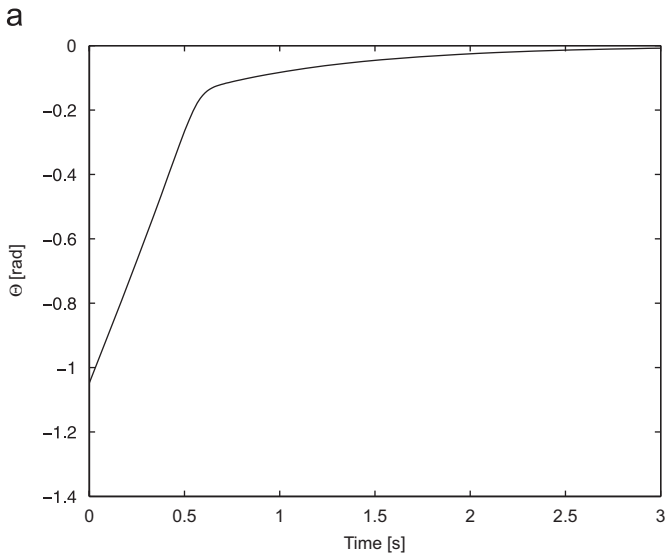

Fig. 22. Time histories of θ and $\dot{\theta}$ of (4.1) under the action of the non-linear controller (8.1), (8.4) with initial conditions $\theta(0) = -\frac{\pi}{3}$ rad and $\dot{\theta}(0) = -1.5$ rad/s. The controller stabilizes the horizontal equilibrium.

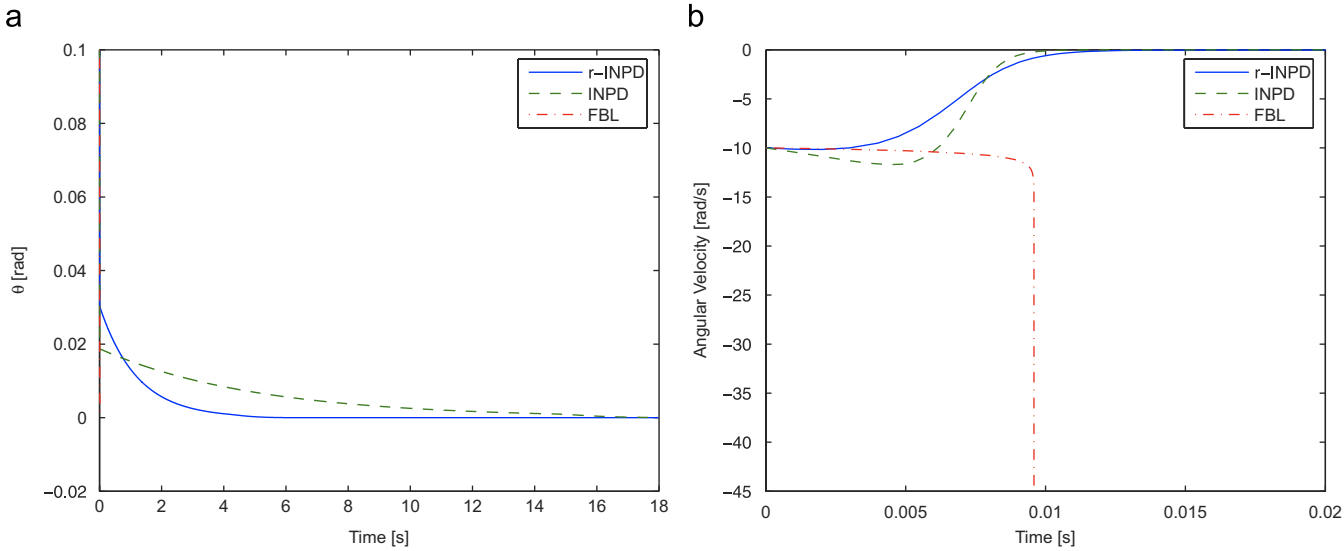

Fig. 24. Time histories of θ and $\dot{\theta}$ of (4.1) under the action of three non-linear controllers, namely, the feedback linearization controller (7.2), the INPD controller (8.3), and the robust INPD controller (r-INPD) (8.4), with a 5% perturbation in mass m. The initial conditions are $\theta(0) = -1.25$ rad and $\dot{\theta}(0) = -10$ rad/s. The feedback linearization controller fails immediately. The robust INPD controller stabilizes the horizontal equilibrium faster than the INPD controller.

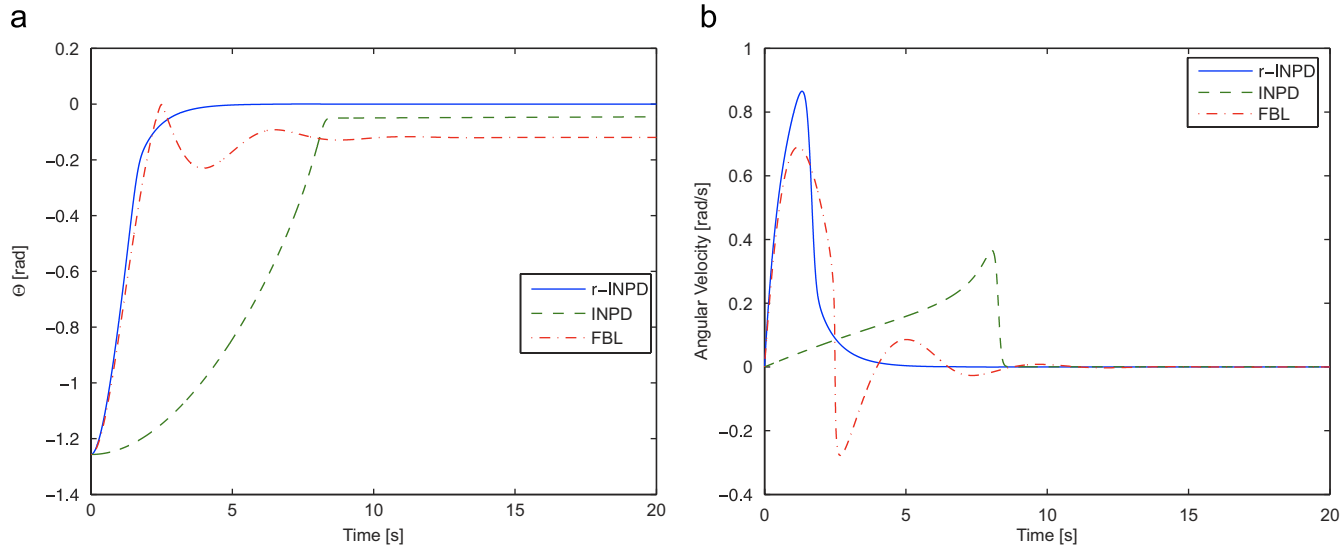

Fig. 25. Time histories of θ and $\dot{\theta}$ of (4.1) under the action of three non-linear controllers, namely, the feedback linearization controller (7.2), the INPD controller (8.3), and the robust INPD controller (r-INPD) (8.4), with a 5% perturbation in the stiffness k. The initial conditions are $\theta(0) = -1.25$ rad and $\dot{\theta}(0) = 0$ rad/s. Only the robust INPD controller stabilizes the horizontal equilibrium.

Note that (8.11) holds for $\theta = 0$ as well as for θ that satisfies

$$\cos\theta = \frac{lk_p}{4kl^2} + \cos\theta_0, \tag{8.12}$$

which is identical to (2.12), where lk_p plays the role of the torsional stiffness k_t. There exists $\theta \in (-\frac{\pi}{2}, \frac{\pi}{2})$ satisfying (8.12) if and only if $lk_p < 4kl^2(1 - \cos\theta_0)$, that is, $k_p < 4kl(1 - \cos\theta_0)$. Since $k_p > 4kl$ in the controller (8.4), it follows that (8.12) has no solution and thus the linkage has exactly one asymptotically stable equilibrium at $\theta = 0$ under the action of the controller. □

The robust-INPD controller (8.4) requires no knowledge of the system parameters other than an upper bound on kl. The gains k_p and k_d in the controller (8.4) are analogous to linear PD gains, and hence the closed-loop response can be modified by adjusting the values of these gains appropriately. Let $m = 1$, $c = 1$ N s/m, $k = 1$ N/m, $l = 1$ m, $k_p = 4.1$ N m, $k_d = 2.5$ N m s, and $\theta_0 = \frac{\pi}{4}$. For the initial conditions $\theta(0) = \frac{\pi}{4}$ rad and $\dot{\theta}(0) = 1$ rad/s, the time histories of θ, $\dot{\theta}$, and control input F are shown in Figs. 20 and 21, respectively. The closed-loop system for the robust INsPD controller converges to the equilibrium $(0, 0)$ in 5 s. These may be compared with results for the

feedback linearization based controller presented in Figs. 15 and 16 for the same initial conditions. As shown, the closed-loop for the robust INPD controller converges faster to the desired equilibrium compared to the feedback linearization controller that takes approximately 15–20 s to converge. Comparing the plots for magnitude of the control input in each case (Figs. 21 and 16), it is seen that the control magnitude for the robust INPD controller is slightly larger (7 N m) than the feedback linearization controller.

Similarly, for the initial conditions $\theta(0) = -\frac{\pi}{3}$ rad and $\dot{\theta}(0) = -1.5$ rad/s, the time histories of θ, $\dot{\theta}$, and the control input F are shown in Figs. 22 and 23, respectively. These may be compared with results for the feedback linearization based controller presented in Figs. 17 and 18 for the same initial conditions. The closed-loop system for the robust INPD controller converges to the equilibrium $(0, 0)$ in 3 s compared to 20 s for the feedback linearization controller. Interestingly, the magnitude of the control actuation for the robust INPD controller (Fig. 23) is less compared to that for feedback linearization controller (Fig. 18). This partly follows from the fact that the robust INPD controller, unlike the feedback linearization based controller, does not cancel any benign non-linearities.

In order to show that the robust INPD controller is indeed robust to inaccurate information of the system parameters, we compare the closed-loop performance using the three different non-linear controllers, the feedback linearization controller (7.2), the INPD controller (8.3), and the robust INPD controller (8.4), respectively. Consider a 5% perturbation in mass m, that is, the mass $m = 1$ kg in the system (4.1), whereas the mass value $m = 0.95$ kg is used in the control laws. Fig. 24 shows the response θ and $\dot{\theta}$ for the three controllers. Note that the feedback linearization controller immediately fails. The robust INPD controller stabilizes the horizontal equilibrium faster than the INPD controller. Similarly, consider a 5% perturbation in stiffness k, that is, the stiffness $k = 1$ N/m in the system (4.1), whereas the stiffness value $k = 0.95$ N/m is used in the control laws. Fig. 25 shows the response θ and $\dot{\theta}$ for the three controllers. Note that only the robust INPD controller stabilizes the horizontal equilibrium.

9. Conclusion

We studied a preloaded two-bar linkage, which serves as a lumped analogue of a structure that can undergo snap-through buckling. We showed that the linkage exhibits hysteresis between the force actuation and the vertical displacement. We also showed that the two-bar linkage with inertialess bars has an inertia singularity and thus is not linearizable at the horizontal (unstable) equilibrium. Finally, we presented the INPD control law as well as the robust INPD control law, which stabilizes the unstable equilibrium with less parametric knowledge of the system.

Acknowledgment

We thank Matthew Cartmell for helpful comments.

References

[1] R. Smith, Smart Materials Systems: Model Development, SIAM, Philadelphia, PA, 2005.
[2] A. Visintin, Differential Models of Hysteresis, Springer, New York, 1994.
[3] D.S. Bernstein, Ivory ghost, IEEE Contr. Sys. Mag. 27 (2007) 21–22.
[4] D. Angeli, J.E. Ferrell, E.D. Sontag, Detection of multistability, bifurcations, and hysteresis in a large class of biological positive feedback systems, Proc. Natl. Acad. Sci. 101 (7) (2004) 1822–1827.
[5] J. Oh, D.S. Bernstein, Semilinear Duhem model for rate-independent and rate-dependent hysteresis, IEEE Trans. Autom. Contr. 50 (2005) 631–645.
[6] D. Angeli, Multistability in systems with counter-clockwise input–output dynamics, IEEE Trans. Autom. Contr. 52 (4) (2007) 596–609.
[7] C.M. Wang, C.Y. Wang, J.N. Reddy, Exact Solutions for Buckling of Structural Members, CRC Press, Boca Raton, FL, 2004.
[8] A. Padthe, J. Oh, D.S. Bernstein, Counterclockwise dynamics of the rate-independent semilinear Duhem model, in: Proc. IEEE Conf. Dec. Contr., Seville, Spain, December 2005, pp. 8000–8005.
[9] in: J.M.T. Thompson, G.W. Hunt (Eds.), Collapse: The Buckling of Structures in Theory and Practice, Cambridge University Press, Cambridge, 1984.
[10] L.N. Virgin, R.B. Davis, Vibration isolation using buckled struts, J. Sound Vibr. 260 (2003) 965–973.
[11] R.H. Plaut, J.E. Sidbury, L.N. Virgin, Analysis of buckled and pre-bent fixed-end columns used as vibration isolators, J. Sound Vibr. 283 (2005) 1216–1228.
[12] M. Yim, D. Duff, Y. Zhang, Closed-chain motion with large mechanical advantage, in: Proceedings of the International Conference on Intelligent Robots and Systems, October 2001, pp. 318–323.
[13] J. Kieffer, J. Lenarcic, On the exploitation of mechanical advantage near robot singularities, Informatica 18 (1994) 315–323.
[14] R.G. Roberts, A.A. Maciejewski, Singularities, stable surfaces, and the repeatable behavior of kinematically redundant manipulators, Int. J. Robot. Res. 13 (1994) 70–81.
[15] S.K. Agrawal, Inertia matrix singularity of series-chain spatial manipulators with point masses, ASME J. Dyn. Sys. Meas. Contr. 115 (1993) 723–725.
[16] F. Ghorbel, M.W. Spong, Integral manifolds of singularly perturbed systems with application to rigid-link flexible-joint multibody systems, Int. J. Non-Linear Mech. 35 (2000) 133–155.
[17] C. Gosselin, J. Angeles, Singularity analysis of closed-loop kinematic chains, IEEE Trans. Robot. Automat. 6 (3) (1990) 281–290.
[18] F.L. Litvin, Z. Yi, V.P. Castelli, C. Innocenti, Singularities, configurations, and displacement functions for manipulators, Int. J. Robot. Res. 5 (2001) 52–65.
[19] E. Zergeroglu, D.D. Dawson, I.W. Walker, P. Setlur, Nonlinear tracking control of kinematically redundant robot manipulators, IEEE/ASME Trans. Mechatronics 9 (2004) 129–132.
[20] S.P. Bhat, D.S. Bernstein, Second-order systems with singular mass matrix and an extension of guyan reduction, SIAM J. Matrix Anal. Appl. 17 (1996) 649–657.
[21] Y. Dumont, D. Goeleven, M. Rochdi, Reduction of second order unilateral singular systems. Applications in mechanics, Z. Angew. Math. Mech. 81 (2001) 219–245.
[22] H.K. Khalil, Nonlinear Systems, second ed., Prentice Hall, New York, 1996.
[23] P.-F. Hsieh, Y. Sibuya, Basic Theory of Ordinary Differential Equations, Springer, New York, 1999.
[24] in: M.P. Mortell, R.E. O'Malley, A. Pokrovskii, V. Sobolev (Eds.), Singular Perturbations and Hysteresis, SIAM, Philadelphia, PA, 2005.
[25] N.A. Chaturvedi, A.M. Bloch, N.H. McClamroch, Global stabilization of a fully actuated mechanical system on a Riemannian manifold: controller structure, in: Proceedings of the American Control Conference, Minneapolis, MN, June 2006, pp. 3612–3617.
[26] A. Padthe, D.S. Bernstein, Hysteresis analysis and feedback stabilization of snap-through buckling, in: Proceedings of the American Control Conference, New York, July 2007, pp. 729–734.

[27] H. Baruh, Analytical Dynamics, McGraw-Hill, New York, 1999.
[28] S.P. Bhat, D.S. Bernstein, Example of indeterminacy in classical dynamics, Int. J. Theoret. Phys. 36 (1997) 545–550.
[29] J. Oh, D.S. Bernstein, Step-convergence analysis of nonlinear feedback hysteresis models, in: Proceedings of the American Control Conference, Portland, OR, June 2005, pp. 697–702.
[30] N.A. Chaturvedi, A.M. Bloch, N.H. McClamroch, Global stabilization of a fully actuated mechanical system on a Riemannian manifold including controller saturation effects, in: Proceedings of the IEEE Conference on Decision and Control, San Diego, CA, December 2006, pp. 6116–6121.
[31] J. Guckenheimer, P. Holmes, Nonlinear Oscillations, Dynamical Systems, and Bifurcations of Vector Fields, Springer, New York, 1983.
[32] G.J. Simitses, An Introduction to the Elastic Stability of Structures, Prentice-Hall, Englewood Cliffs, NJ, 1976.